NDT&E International 154 (2025) 103378

Contents lists available at ScienceDirect

NDT and E International

journal homepage: www.elsevier.com/locate/ndteint

FMCW THZ radar and X-ray analysis of wood properties: A comparative study

Caroline Marc *, Bertrand Marcon, Louis Denaud, Stéphane Girardon

Arts et Metiers Institute of Technology, LaBoMaP, HESAM Université, Cluny, F-71250, France

ARTICLE INFO

Keywords:
Wood
Terahertz
FMCW radar
Local density
X-ray

ABSTRACT

Wood is a material valued for its mechanical properties and sustainability. It exhibits substantial variability in density due to its growth being influenced by the external environment. The measurement of its local properties is therefore crucial for various applications such as in the construction and transport industries. X-ray attenuation densitometry measurement is a well-established method, but it uses ionizing radiation which can pose hazards to human health. Its cost is significant in terms of investment and consumables. Terahertz (THz) technology, being non-ionizing and promising, emerges as an alternative for density imaging. Therefore, this study employs THz frequency modulated continuous wave (FMCW) radar, a novel approach, to assess its ability to predict local density in a pool of 110 samples from diverse wood species, with different thicknesses, and a wide density range (from 111 kg m^{-3} to 1086 kg m^{-3}) representative of the natural variability of wood density — both at the local scale of growth rings and at a global scale. The beating signal of the FMCW radar was modeled by considering the crossed medium as uniform, to extract both the optical index and the absorption coefficient. Additionally, the local density was measured using an X-ray industrial timber scanner as a reference for the actual local density. Results reveal strong correlations between density and THz parameters. However, the study highlights limitations in the THz modeling, such as wood vessel scattering, thickness influence, potential polarization effect, or non-uniformity of the medium between earlywood and latewood.

1. Introduction

Wood is a material with promising mechanical properties and sustainability, making it a commonly used resource in various industries. However, this natural material is known for its substantial variability. Several factors, including the tree's growth conditions, for example, play a crucial role in shaping the wood's physical attributes and among others its mechanical characteristics. Density is one of these attributes [1]. While the density of the wood cell wall consistently averages between around 1400 kg m^{-3} and 1500 kg m^{-3} across wood species [2], variations in wood density stem from differences in cell size and cell wall thickness (the ratio of cell wall to air), resulting in a density range of approximately 100 to 1200 kg m^{-3}. Measuring it locally is therefore relevant to predict wood behavior and determining its suitability for various applications.

Several non-destructive techniques have been explored for wood density measurement, among which ultrasonic testing has been widely investigated due to its effectiveness and affordability. Ultrasonic methods rely on the propagation of acoustic waves, whose velocity is influenced by the wood's density and microstructure. Multiple studies have demonstrated a strong correlation between ultrasonic wave velocity and wood density across various species [3,4]. These techniques can be applied either in contact or using air-coupled transducers, making them versatile for industrial applications [5]. However, their accuracy can be affected by several factors, including wood anisotropy, moisture content, and the need for proper sensor coupling [6]. Additionally, while ultrasonic equipment is significantly more affordable than X-ray or terahertz systems [7], its spatial resolution remains limited, typically in the range of several millimeters [7,8].

Local non-destructive measurement of wood density can also be achieved through X-ray attenuation measurement. X-ray technology provides a very high level of accuracy and spatial resolution for density measurement (on the order of 0.1–10 nm). X-ray are already widely studied for this application [9–12] and used in various industries. The main drawback of this method is the ionizing nature of this range of radiation, which poses potential health risks and industrial implementation issues (when close to operators and for exploitation and maintenance). This is where terahertz (THz) technology emerges as a

* Corresponding author.
E-mail address: Caroline.Marc@ensam.eu (C. Marc).

https://doi.org/10.1016/j.ndteint.2025.103378
Received 19 December 2023; Received in revised form 3 March 2025; Accepted 5 March 2025
Available online 6 March 2025

promising alternative. While not as extensively researched as X-ray, THz technology presents distinct advantages as it is non-ionizing and therefore harmless [13,14] and holds substantial potential for wood density imaging. The THz domain, residing between the realms of infrared and microwave frequencies, encompasses electromagnetic waves with frequencies ranging from 0.1 to 10 THz. The wavelength of these radiations allows them to penetrate a wide variety of non-conductive materials, including wood, while providing spatial resolution on the order of millimeters (from 0.03 mm to 3 mm).

Due to the scientific challenges involved in generating and detecting THz waves, it wasn't until the 1980s that these waves became commonly studied and subsequently utilized [15]. Hence, this is a relatively recent field of study. However, it is a rapidly advancing field, and the advantages of these radiations make them excellent tools for non-destructive testing and wood imaging. Koch et al. [16] were among the pioneers in providing wood density maps with a sub-annual ring resolution, using THz transmission and Beer-Lambert's law [17]. Tanaka et al. [18] conducted measurements in the THz range (from 0.15 to 1.2 THz) to determine wood's dielectric properties, demonstrating a clear correlation between the oven-dry density of wood and its dielectric properties. These properties were determined by applying the effective medium theory, which consists, in this case, of considering wood as a mixture of dry cell wall material, air and water. Inagaki et al. [19] employed a similar approach and was able to extract the real and imaginary parts of the complex dielectric function of the samples averaged over the frequency range of 0.1–0.2 THz, and predict not only the density but also the moisture content (MC). Their study encompassed four wood species, and they achieved remarkable predictions of wood density, ranging from approximately 360 to 800 kg.m-3, with a high correlation coefficient (R^2) of 0.98 when measurements were made with the polarization of the THz field perpendicular to the wood grain, and 0.96 when parallel. Indeed, as wood is a fibrous material, at different scales ranging from micrometric to millimetric one as for the THz millimetric wavelengths, it is essential to consider the polarization of the radiation. The birefringence of wood, an optical property where the refractive index depends on the polarization direction, has enabled Kashima et al. [20] to measure the refractive index and the absorption coefficient, and to deduce the fiber's orientation. By applying these values along with multiple linear regression, they accurately predicted wood density (R^2 = 0.97) and MC.

All these measurements, who showed great potential, were made using THz time domain spectroscopy. In this study, the THz measurement will be made with a frequency modulated continuous wave (FMCW) radar, which is a type of radar system that continuously transmits a periodic signal with varying frequency to detect and measure the velocity and distance of objects and was never studied as a wood density measurement tool before. The objective is to evaluate the capacity of THz FMCW radar measurement to predict local density of 110 samples with a wide range of wood species and densities, ranging from 111 kg m^{-3} to 1086 kg m^{-3}, and to use X-ray density measurement as the reference value.

2. Materials and methods

2.1. Samples

Scanning procedures were conducted on a total of 110 samples, all measuring 130 mm × 60 mm but varying in thickness from 1 to 10 mm. These samples were subsequently divided into two distinct groups, which will be referred to as the 'Diverse group' and the 'Tropical group' in this study.

The "Tropical group" consists of 32 samples obtained from a xylotheque (library of wooden samples well identified and stored) of tropical hardwoods from Africa and Asia, with a thickness of 9 ± 1 mm. The 32 species are as follows: Aiele (*Canarium schweinfurthii*), African mahogany (*Khaya anthotheca*), Ako (*Antiaris toxicaria*), Avodire (*Turraeanthus Africanus*), Azobe (*Lophira alata*), Bete (*Mansonia altissima*), Bosse (*Guarea cedrata*), Bubinga (*Guibourtia demeusei*), Dau (*Xylopia* spp.), Dibetou (*Lovoa trichilioides*), Doussie (*Afzelia Africana*), Framire (*Terminalia ivorensis*), Ilomba (*Pycnanthus angolensis*), Iroko (*Milicia excelsa*), Kossipo (*Entandrophragma candollei*), Kotibe (*Nesogordonia papaverifera*), Limba (*Terminalia superba*), Makore (*Tieghemella africana*), Niangon (*Heritiera utilis*), Niove (*Staudtia kamerunensis*), Okoume (*Aucoumea klaineana*), Olon (*Fagara heitzii*), Ozigo (*Dacryodes buettneri*), Rosewood (*Dalbergia* spp.), Cam Laï Rosewood (*Dalbergia* spp.), Rosewood Trac (*Dalbergia cochinchinensis*), Samba (*Triplochiton scleroxylon*), Sapelli (*Entandrophragma cylindricum*), Sipo (*Entandrophragma utile*), Teak (*Tectona grandis*), Tiama (*Entandrophragma angolense*), Zingana (*Microberlinia bisulcata*). The samples were obtained from cuts that varies between radial and tangential orientations (cf. Fig. 1-(a)).

The "Diverse group" consists of 78 samples that were specially manufactured for the study, utilizing six distinct wood species: balsa (*Ochroma pyramidale*), beech (*Fagus sylvatica*), red cedar (*Thuja plicata*), Douglas fir (*Pseudotsuga menziesii*), poplar *(Populus Tremula*), and oak (*Quercus Robur*). These samples were also sourced from wood cuts that vary between radial and tangential sections, with the exception of the Douglas fir samples, which were subdivided into two subcategories: radial cut and tangential cut. The samples come in three different thicknesses: 1 mm, 3 mm, and 5 mm. Each combination of wood species and thickness (and cuts, in the case of Douglas fir) is replicated four times, except for the 1 mm thick samples of poplar, radial Douglas fir, and tangential Douglas fir, which are each replicated only twice.

To facilitate alignment between different measurement methods (THz and X-ray scans), the samples were drilled with through holes measuring 6 ± 0.1 mm in diameter, located at three of their corners, as depicted in Fig. 1-(b).

2.2. Measurement

2.2.1. Local density X-ray measurement

The average density of each sample is known by weighing and measuring their external dimensions. But to be able to compare the THz wave measurements to density values at any point of the samples, their local density was measured with an industrial optical scanner equipped with, among other features, an X-ray transmission imaging system. This process generated two-dimensional maps with a 12-bit grayscale range (ranging from 0 to 4095 Gy levels). The grayscale levels are directly proportional to the intensity of transmitted X-ray I ($Sv.h^{-1}$), and therefore related to the density ρ ($kg.m^{-3}$) according to the Beer-Lambert's law (equation (1)) [17], with μ the attenuation coefficient of the material ($m^2.kg^{-1}$), d the thickness of the sample (m), and I_0 the intensity of the incident radiation ($Sv.h^{-1}$).

$$\rho = \frac{1}{\mu \bullet d} \log\left(\frac{I_0}{I}\right) \tag{1}$$

Assuming that the coefficient μ is the same for all samples of the same species and knowing that the gray levels obtained following the measurement are proportional to the intensity of the wave transmitted, the relationship between gray level (GL) and density is written according to equation (2). Since samples of the "Tropical" group are all of a different species, a μ common to all will be considered. This last hypothesis will be discussed in results and discussion section thanks to measurements.

$$\rho \bullet d = a \bullet \ln(GL) + b \tag{2}$$

The values of parameters a and b are identified using pairs of values (gray level, $\rho \bullet d$) that are already known. The values of gray level and thickness are known at any point, assuming that the thickness is the same on the whole sample, while the average density for each sample is the only available information. A linear regression is therefore performed on the values of the product of the average density by the thickness according to the average of the logarithms of the gray levels

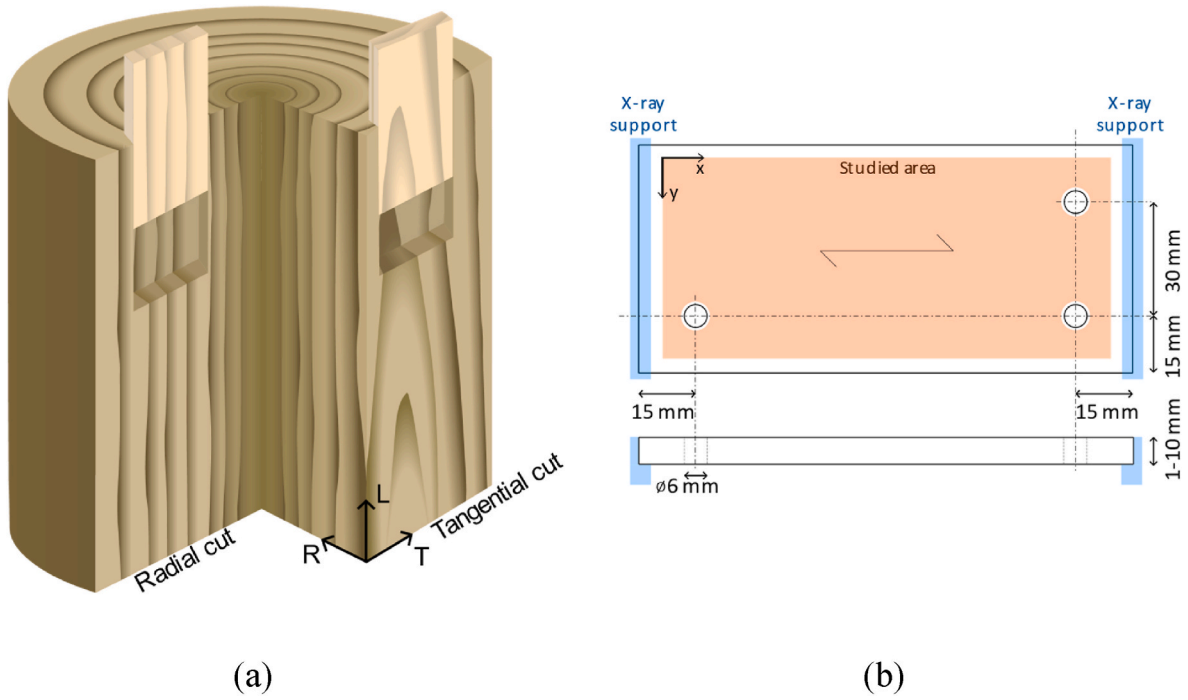

Fig. 1. (a) direction and cut of wood, with a radial sample and a tangential sample, (b) sample dimensions; the three through-holes are performed to avoid any inaccurate localization between X-ray and THz scans and to help overlap both scan data sets.

per sample.

The X-ray source's settings were optimized beforehand (35 kV, 35 mA) to ensure that the images didn't suffer from saturation, neither in dark nor in bright regions. These images have a spatial resolution of 1 mm.px^{-1} along the grain direction (the length of the samples) and 0.34 mm.px^{-1} in the perpendicular direction (width of the samples).

As the scanner is primarily designed for assessing boards, the samples required a support during the scanning process. This support caused distortion in the transmitted intensity where the samples are held on the support, along a strip of approximately 2 mm at both ends of the samples (as shown in Fig. 1-(b)).

2.2.2. *Frequency modulated continuous wave terahertz radar*

Measurements at THz frequencies were performed using a FMCW radar (Terascan 100, Lytid). The operating of the FMCW radar measurement [21], illustrated in Fig. 2 is the following: a signal is emitted by a voltage-controlled oscillator, with a progressively varying frequency (from 110 GHz to ~130 GHz) due to a triangle modulation. This signal is multiplied in frequency and then transmitted to a target through the transmitting antenna. A portion of this signal is reflected back by the target, which corresponds to an interface between two media with

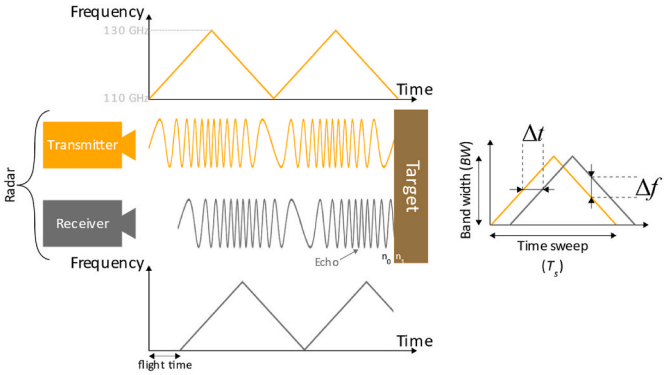

Fig. 2. Operating principle of a FMCW radar.

different optical indices. The proportion of reflected signal depends, among other things, on the go through optical indices. The reflected signal is then received and combined with the emitted signal to produce the beating signal. The frequency of this signal (Δf in Fig. 2) is proportional to the round-trip distance between the radar and the target. If the signal encounters multiple targets on its path (e.g., irregularities in the sample or the backside of the sample), the beating signal can be decomposed into as many sinusoids as there are interfaces. Each sinusoid has a frequency related to the interface to radar distance. By analyzing the beating signal, information on the media with which the wave has interacted can be obtained, as well as the position of these media relative to the radar.

equation (3) gives the relation between the beating signal frequency (Δf) and the distance to the target (z) [22]:

$$z = \frac{c \bullet \Delta t}{2n} = \frac{c \bullet \Delta f \bullet T_s}{2n \bullet BW} \tag{3}$$

with c the speed of light (m.s^{-1}), Δt the time delay between emitted and received signal (s), n the optical index of the propagation medium (−), Ts the sweep time (283.889 µs) and BW the sweep bandwidth (19.505 GHz). The assumption is made that the refractive index of air (n_{air}) is strictly equal to 1 [23].

Prior to measuring the samples, radar calibration is conducted. Initially, measurements are taken of the background, followed by measurements of a reference point using a metallic mirror positioned at the focal point of the optical setup. These reference points serve to filter optical-related noise, and its plane is established as the zero-beating frequency reference. During the measurements, the samples are placed on this mirror, which has been displaced from the radar by a distance equivalent to the thickness of the sample being assessed. This positioning ensures that the focal point aligns with the first face of the sample that the waves encounter. The scans exhibit a spatial resolution of 1 mm.px^{-1} in both plan directions namely x and y (in Fig. 1-(b)).

The THz wave is polarized in the direction of the sample width (y direction in Fig. 1-(b)).

2.2.3. Measurement of dimensions and moisture content

The dimensions of the samples (length, width and thickness) were measured using a digital caliper (resolution 0.01 mm). Their mass was measured using a Kern balance (resolution 0.01 g) shortly before the THz and X-ray measurements. The overall density was calculated based on this data, while considering the missing volume due to the drill holes.

The samples were not humidity-stabilized in a climatic chamber prior to measurement, but simply left in ambient air assuming that their humidity was stabilized to the ambient conditions in the laboratory as the duration of THz measurement (approximately 40 min per specimen) cannot ensuring the non-variation of moisture content in the specimens. After the scans, the samples were placed in a climatic chamber set at 30 °C and 50 relative humidity, and their masses ($m_{9\%}$) were recorded at 9 % of equilibrium MC ($MC_{9\%}$) which was close to the supposed equilibrium MC in ambient conditions. Based on these measurements and knowing the mass of the samples at the time of the X-ray and THz scans (m_t), their overall MC at the time of the measurements (MC_t) could be obtained using equation (4) using the definition of MC [24].

$$MC_t = MC_{9\%} + \frac{m_{9\%} - m_t}{m_{9\%}}(1 + MC_{9\%}) \tag{4}$$

2.3. Signal processing

2.3.1. Preliminary radar data processing

The data obtained from the radar scans of the samples consist of temporal signals, with one signal acquired every 1 mm^2. To process these data, some preliminary quite usual signal treatments must first be done, and in particular to place oneself in the frequency domain, to be able to focus on the frequency range that concerns the interactions with the sample. To begin with, a Hamming's window function is applied to the signal in order to avoid spectral leakage and damp its extremities towards 0 in order to perform a zero-padding [25]. This operation is used to improve the longitudinal resolution (tangential direction of the wood) in distance. Indeed, the sampling frequency is $Fs = 1.8$ MHz, which allows obtaining 512 values per signal. Thus, after going into the frequency domain, the frequency resolution is obtained by dividing Fs by 512. According to equation (3), this corresponds to a distance resolution of approximately 7.7 mm (with $n = 1$), which is within the same order of magnitude as the samples thickness which can lead to interference issues. The zero-padding allows the artificially increasing of this resolution by adding zeros at the end of the temporal signal, which increases the number of samples, while keeping the same frequency band (Fs) and without adding information. A zero-padding factor of 64 is used here, which gives a frequency resolution of Fs divided by 512 × 64, corresponding to a frequency resolution of 54.9 Hz and 0.12 mm in distance, thus much more consistent with the dimensions of the measured elements. Following zero-padding, the signal undergoes a fast Fourier transform (FFT) and is subsequently normalized by dividing it by the maximum absolute value of an array of size 64 × 512 having undergone the same operations as the signal (windowing, zero-padding then FFT). The resulting normalized signal corresponds to the ratio of the received signal to the transmitted signal, also called transfer function.

2.3.2. Extraction of the parameters of the crossed environment

The beating signal contains information about the media that the radar wave has crossed. Among this information, the parameters that will be studied to determine their relationship with density are the optical index n (dimensionless) and the absorption coefficient α (cm^{-1}). To calculate these two parameters at all points of the samples (1 mm^2 resolution), the methodology used here will be to model the beating signal as a function of n and α, and then find the pair of values of n and α that produce the theoretical signal that is most similar to the experimental signal. In this study, two assumptions have been made to simplify the modeling. The first assumption is that the samples have two flat and parallel sides and are uniform in the transverse direction, meaning that n, α, and ρ are constant across the sample thickness. The second assumption is that the THz wave-matter interactions such as refraction, scattering, and diffraction are negligible in the studied case and therefore not considered in the modeling, unlike reflection and attenuation.

The formula for the beating signal is written according to equation (4) [26], where p represents the number of interfaces, r_i is the amplitude coefficient, τ_i is the time of flight, and Δf_{min} is the first frequency emitted during the sweep (110 GHz). As shown in Fig. 3, it will be considered that $p = 3$, with the first two interfaces representing the front and back sides of the sample, and the third interface representing the back side once the wave has completed a round trip through the sample. Because of the attenuation of the medium through which they pass, the following interfaces have only a very limited effect on the final amplitude, and will therefore not be considered.

$$S_b(t) = \sum_{i=1}^{p} r_i e^{j2\pi\left(\Delta f_{min}\tau_i + \frac{BW}{T_s}\tau_i t\right)} \tag{4a}$$

The values of τ_i and r_i are determined using equations (5) and (6), respectively. The amplitude coefficients of the beating signals correspond to those of the reflected signals at the three interfaces, namely $S_r(t)$, $S_{trt}(t)$ and $S_{trrrt}(t)$ shown in Fig. 3. These coefficients are calculated using formulas that consider the Fresnel's coefficients for reflection (r_{i_j}) and transmission (t_{i_j}) explained in equations (7) and (8), respectively. Since metal is totally reflective of THz, r_{wood_metal} is taken to be equal to 1. Additionally, the influence of absorption is considered based on the Beer-Lambert's law (equation (1)).

$$\begin{aligned} \tau_1 &= 0 \\ \tau_2 &= 2 \bullet d \bullet n_{wood}/c \\ \tau_3 &= 4 \bullet d \bullet n_{wood}/c \end{aligned} \tag{5}$$

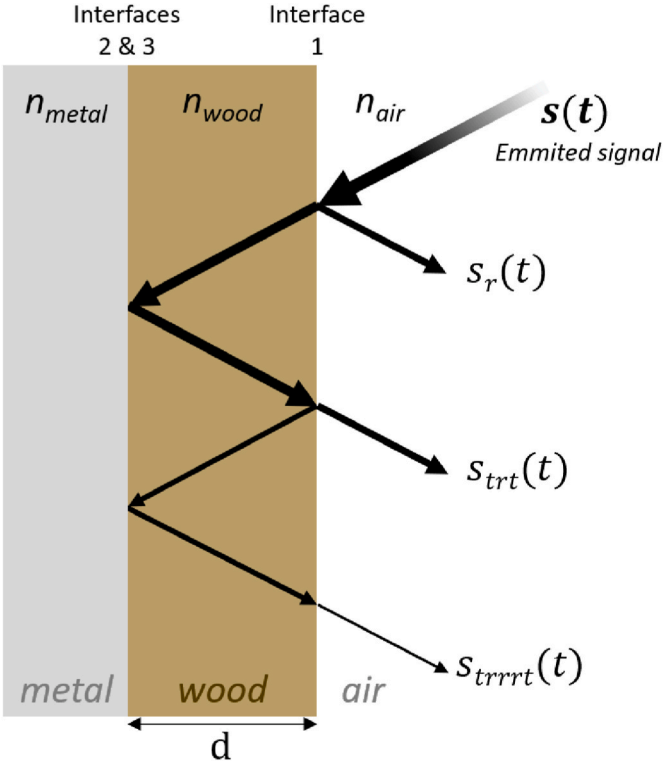

Fig. 3. Signal path diagram.

$$\begin{aligned} r_1 &= r_{air_{wood}} \\ r_2 &= t^2_{air_{wood}} \bullet r_{wood_{metal}} \bullet e^{-2\alpha d} \\ r_3 &= t^2_{air_{wood}} \bullet r^2_{wood_{metal}} \bullet r_{wood_{air}} \bullet e^{-4\alpha d} \end{aligned} \tag{6}$$

$$r_{i_j} = \frac{n_i - n_j}{n_i + n_j} \tag{7}$$

$$t_{i_j} = \frac{2}{n_i + n_j} \tag{8}$$

The theoretical signal is generated using the same sampling frequency as the experimental signal, then the preliminary processing detailed in subsection 2.3.1 is applied to it. Finally, the modeled depends on 3 variables: the sample thickness d, which is known, the optical index n, and the absorption coefficient α.

As previously mentioned, the n and α of the medium can be determined by comparing the theoretical and experimental signals. To achieve this, the function described in equation (9), being the root mean square error (RMSE) between the amplitude of the two signals (with n and α as parameters), is then minimized to approach the theoretical model to the experimental signal as much as possible considering the initial simplifications enumerated before avoiding the perfect correspondence but still exhibiting great agreements.

The observed signal is not observed in its entirety, and a sample size T of 200 is taken, which corresponds to the first 200 samples starting from the zero-beating frequency. This sample size corresponds to a 14 mm distance, which includes the part of the signal reflected at the first interface as well as the part reflected at the third interface, even for the thickest samples.

$$RMSE(n,\alpha) = \sqrt{\frac{\sum_{t=1}^{T}\left(|S_b(n,\alpha)|_t - |S_{b\_exp}|_t\right)^2}{T}} \tag{9}$$

2.4. X-ray – THz maps alignment

To compare the mappings obtained by the two measurement methods, the density (X-ray) mappings must first be downsampled to a resolution of 1 mm.px^{-1} in both dimensions using average method, to match the mappings obtained using the THz radar. During measurements, especially in the case of THz radar, significant edge effects occur at the periphery of the samples, making precise localization challenging down to the millimeter level. Additionally, it's possible that the edges of the samples may not align perfectly with the reference frame against which they were scanned. For these two reasons, as mentioned earlier, the samples are equipped with holes that serve as reference points for aligning the mappings obtained by both measurement methods. Once the positions of the three holes are manually detected in both cases, an affine transformation is applied to the density mappings to align them. Lastly, as illustrated in Fig. 7, the pixels within an 8-pixels diameter circle centered on the holes will not be considered to ensure that areas without wood and the resulting edge effects are not taken into account in the comparisons.

3. Results and discussion

3.1. X-ray

As previously mentioned, the relationship between transmitted X-ray signal intensity and density is determined performing a linear regression between, on one hand, the product of actual density and thickness, and on the other hand, the average of the logarithms of the grayscale levels, based on Beer-Lambert's law. The correlation coefficients (R^2) for these regressions are displayed by wood species in Fig. 4-(a). All R^2 values indicate a strong correlation. The R^2 for the Tropical wood group is slightly lower than the others (96.4 %), which can be explained by the fact that all the samples are from different wood species, and the attenuation coefficient μ significantly varies from one species to another. Fig. 4-(b) illustrates the relevance of X-ray measurements when grayscale values are converted into density units, exhibiting a strong correlation of 98.9 % between actual average density and that derived from X-ray measurements for each sample. The second column of Fig. 7 presents density maps of six samples, distinctly revealing growth rings.

3.2. Result of the THz signal modeling

The outcomes of the optical parameters extraction from the THz beating signal are presented through the subsequent three figures.

Fig. 5 allows observing, for a given point of a 5 mm thick Douglas fir sample and a 5 mm thick poplar sample, the amplitude of the measured beating signal, as well as the amplitude of the beating signals modeled according to the method described in subsection 2.3.2, with $p = 3$. The figure also includes the amplitude of the beating signals obtained by considering in the modeling a number of interfaces p encountered by the

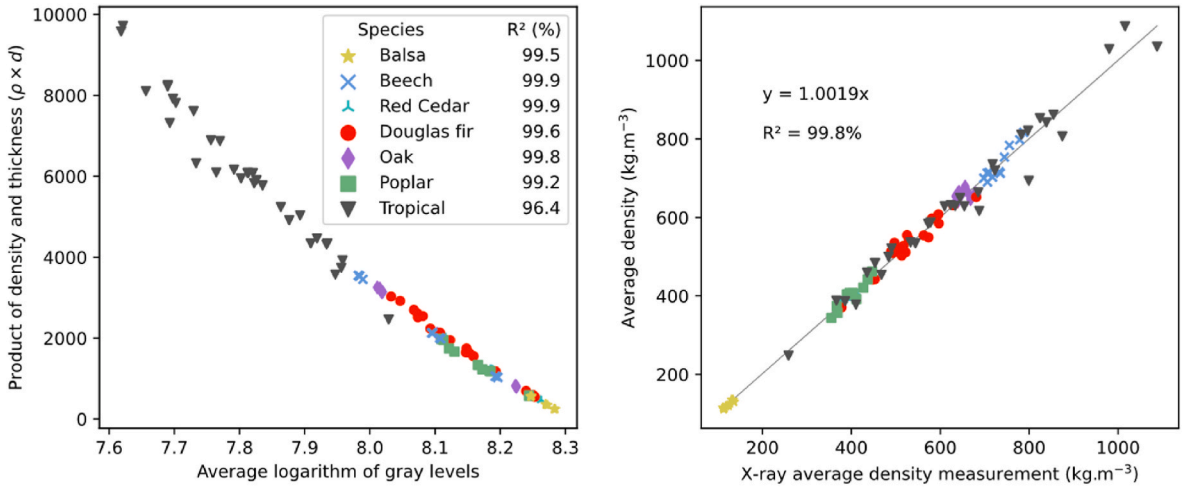

Fig. 4. X-ray density measurement: (a) Identification of a and b parameters, and (b) average measured density versus average X-ray density.

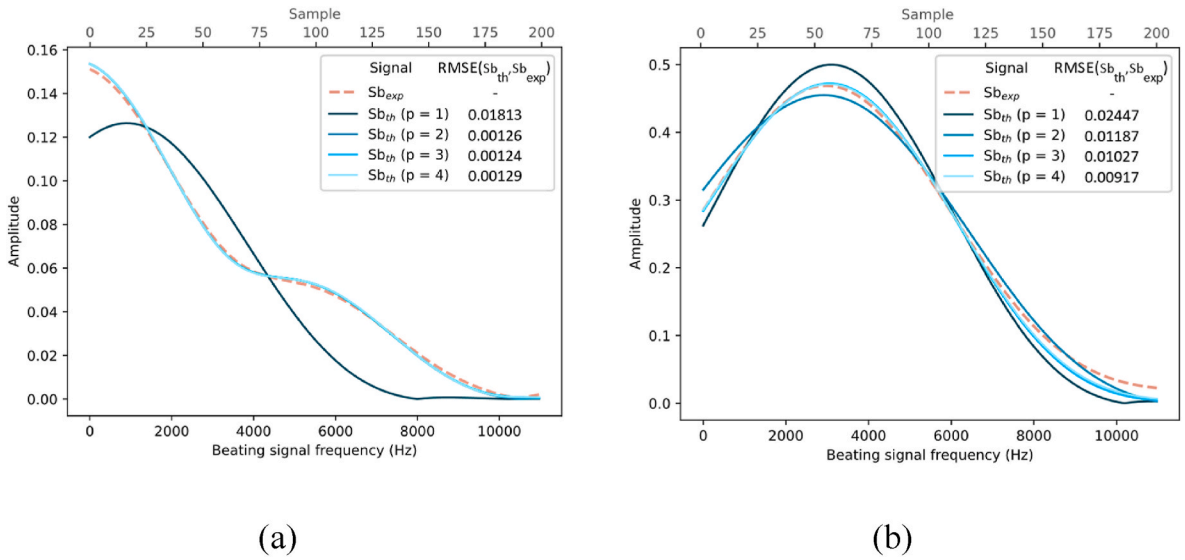

Fig. 5. Amplitude of the experimental beating signal (Sb_{exp}) and signals modeled (Sb_{th}) with $p = 1$ to 4 interfaces by minimizing the RMSE according to equation (9), measured on a 1 mm^2 point of: (a) a 5 mm thick radial Douglas fir sample, and (b) a 5 mm thick poplar sample.

wave equal to 1, 2, and 4, to see the influence of the number of interfaces considered on the result of the RMSE minimization. In the case of Fig. 5-(a), a clear difference is visible between the modeling with $p = 1$ and the others, which seems normal because it only considers the reflection at the first face of the sample. The other curves, with $p = 2$, 3, and 4, are almost identical. This means that 2 interfaces could be sufficient here to represent the behavior of the wave through the sample. However, in the case of less dense wood, the third interface tends to have a more significant influence since the wave is less attenuated as it passes through the wood. For example, here with poplar in Fig. 5-(b), the curve with $p =$ 3 and 4 are also almost indistinguishable, but it is not the case for the curve with $p = 2$, which is slightly less similar to the amplitude of the experimental signal.

Fig. 6 illustrates the mean value per sample of the RMSE function's minimum, as defined in equation (9), with respect to the actual density. Fig. 7 presents maps originating from both X-ray (density) and THz (absorption coefficient, optical index, and RMSE) measurements, along with a photograph of the sample, for 3 samples from the "Diverse" group and 3 samples from the "Tropical" group. At first sight, it is possible to observe that for most of the samples, the maps exhibit similarities between X-ray and THz measurements, suggesting a robust consistency in the employed beating signal model. The average RMSE values, ranging from 0.002 to 0.015 and thus very close to 0, indicate a high level of precision in the model's predictions. To put this into perspective, if we

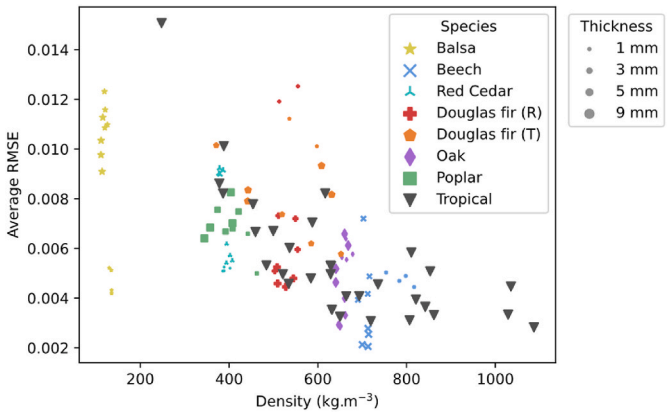

Fig. 6. Average RMSE per sample as a function of density.

were to calculate the mean RMSE across all samples, employing parameters such as $n = 1.4$ and $\alpha = 0.5$ cm^{-1} for the theoretical beating signal, the resulting value would be 0.092, markedly higher than the optimized values.

Fig. 6 reveals a pattern between RMSE and density: denser samples tend to exhibit lower RMSE values, implying more accurate predictions in contrast to their less dense counterparts. This trend can also be observed within a single sample, for example with the dibetou wood in Fig. 7, where the growth ring pattern corresponds to the RMSE mapping. This observed correlation could potentially be explained by the relationship between wood density and refractive index. Specifically, as wood density increases, so does its refractive index. Consequently, the amplitude of the signal transmitted at the first interface diminishes for denser wood in comparison to less dense varieties. As a reminder, the modeling considers the summation of three signals: one signal reflected at the first interface, another reflected at the second interface, and a third reflected at the second interface after an additional round trip between the two faces. Among these three signals, the first signal has a higher amplitude for denser wood compared to less dense wood, while the two subsequent signals, having traversed the sample where phenomena other than reflection and attenuation may have occurred, exert a more pronounced influence on less dense wood. In summary, lower sample density results in the assumptions outlined in subsection 2.3.2 being less applicable, thereby explaining the higher RMSE.

Most of the THz maps follow the growth ring pattern; however, in some cases, such as Douglas fir, it appears that there are more features than rings. This anomaly could be attributed to pronounced density variations between earlywood and latewood (280 kg m^{-3} and 750 kg m^{-3} for Douglas fir), giving rise to interfaces between distinct optical material properties. These interfaces may introduce edge effects, potentially causing inaccuracies in measurements within these regions.

Furthermore, the presence of measurement artifacts should not be overlooked. For example, in the case of Dibetou, small irregularities on THz maps are imperceptible on the RX one, and remain invisible to the naked eye when examining the sample directly. On a larger scale, some absorption coefficient and refractive index maps reveal patterns that deviate significantly from the expected wood growth rings. This anomaly is evident in Fig. 7 for oak, zingana, and bosse samples, with these unusual patterns appearing consistently in oak samples and across almost all 'Tropical' group samples. The common feature among the studied tropical species and oak is the diameter of their vessels, which is approximately 100 μm or more [27], significantly larger than that of

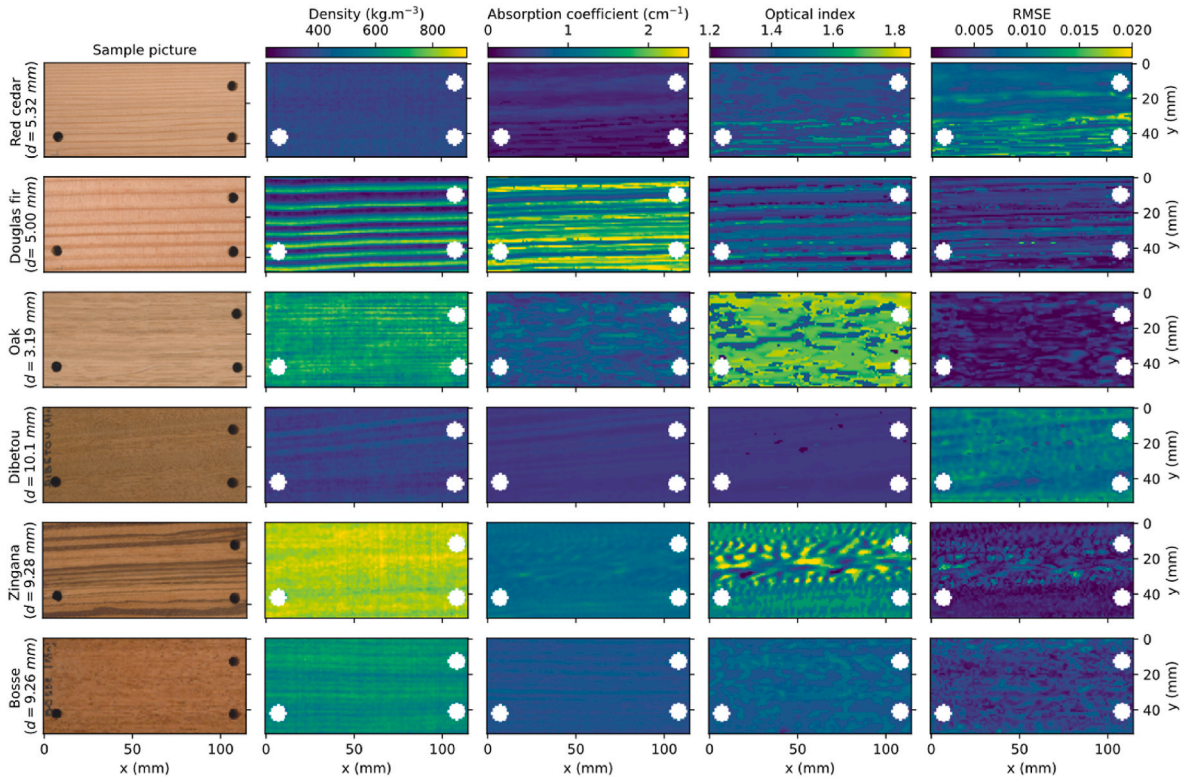

Fig. 7. Photograph of 6 samples of different species and their mapping in X-ray density, absorption coefficient, optical index and RMSE between the amplitude of the experimental and theoretical signal (equation (9)).

other species with vessels. Moreover, Tanaka [18] demonstrated that waves with wavelengths ranging from 250 µm to 500 µm are scattered by wood vessels with similar dimensions, and Sihvola [28] enunciated the following rule of thumb often employed: "the size of an inclusion in the mixture must not exceed a tenth of the wavelength in the effective medium". In this study, the wavelengths used range between approximately 2300 µm and 2500 µm, which is about 10 times larger than the pore diameters. This leads to the observation that cavities formed by vessels with diameters exceeding 100 µm are of sufficient volume to interact with the THz waves used in this study, rendering unrealistic the assumption that the wave propagates through a continuous medium during its journey through the sample. The tropical samples that do not exhibit these interaction patterns (balsa, dibetou, ilomba, samba) happen to be the least dense in the group ($\rho < 400$ kg/m^3). If these interactions are not visible for samples characterized by large vessels but low density, this may be explained by the fact that the lower the wood density, the closer its refractive index is to that of air in theory, thereby minimizing interactions at the interface.

While features on the order of a tenth of a millimeter may exert some influence on measurements, it becomes apparent that details of 2 mm in size, equivalent to the wavelength used, or smaller, are no longer clearly discernible on the mappings. This phenomenon is particularly evident in the case of the Red Cedar sample, where the growth rings gradually converge from one side to the other. On the THz maps, the rings are discernible on just one side of the sample when spaced more than 2 mm apart. An additional intriguing observation regarding this sample is that these rings are tilted at an angle of 70.4° relative to the incident wave direction (see Fig. 10), in addition to being closely spaced, which accounts for their absence in the X-ray maps. The fact that they can be observed on the THz maps once again underscores that the employed modeling is not perfectly suited for this set of samples.

3.3. Correlation between average THz optical parameters and global density

Fig. 8(a) and 8(b) present a sample-wise comparison between the optical index (n), the absorption coefficient (α), and the actual density (ρ). The optical index and absorption coefficient values employed in this comparison are the previously mentioned values, averaged per sample. One notable observation is that the thickness of the samples exerts an influence on the obtained THz optical parameters. Within the same wood species, and therefore for samples with similar densities, the optical index tends to increase as thickness decreases, while the absorption coefficient decreases with increasing thickness. This once again suggests that the modeling is not optimal, as thickness is accounted for in the beating signal formula and should not cause variations in the optical parameters of the samples, and that the microstructure disturbs the wave propagation in a non-linear way.

To mitigate the impact of thickness, the relationship between the mean optical index, mean absorption coefficient, and density was separately examined for each thickness category. Table 1 thus presents the correlation coefficients between the RX and THz values, along with their corresponding p-values, for the four thickness categories. Whether in Table 1 or Fig. 8, it is obvious that the correlation is stronger for the

Table 1
Correlation coefficients and p-values of linear regression between average optical index and density, and average absorption coefficient and density, by thickness.

	$\rho = f(n)$		$\rho = f(\alpha)$	
Thickness	R^2 (%)	p-value	R^2 (%)	p-value
~9 mm	97.1	≪0.01	77.8	≪0.01
5 mm	92.1	≪0.01	44.1	≪0.01
3 mm	72.3	≪0.01	38.4	≪0.01
1 mm	17.2	0.054	10.2	0.148

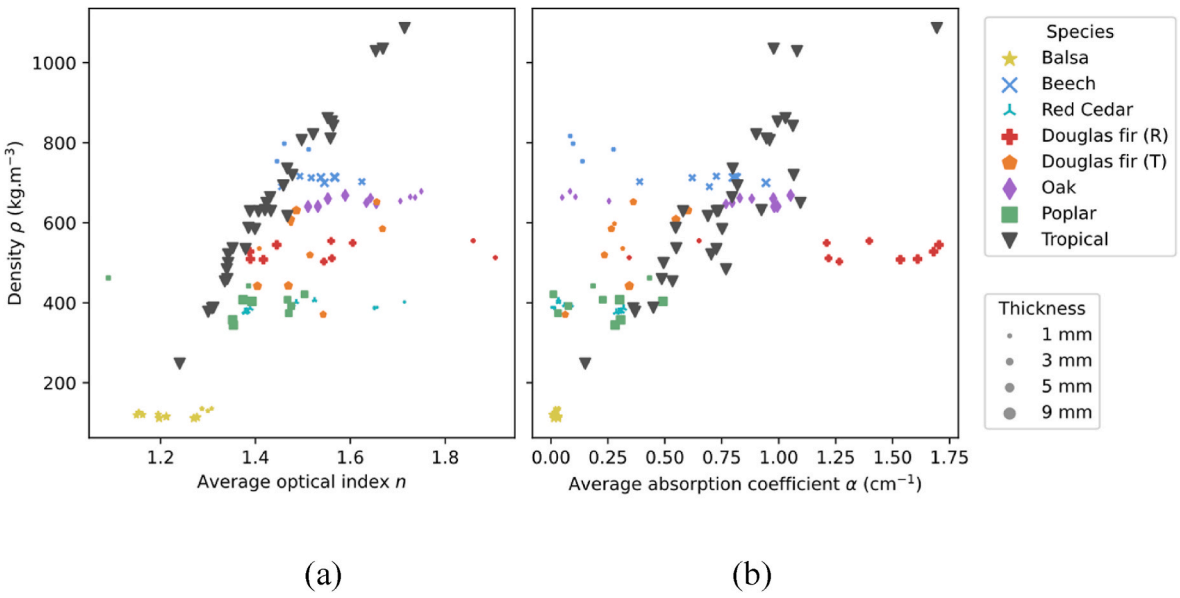

Fig. 8. Density as a function of (a) Average optical index, (b) Average absorption coefficient.

thicker samples, particularly regarding the optical index of tropical samples, which exhibits a remarkable R^2 of 97.1 %. The correlation between α and ρ is generally weaker than that between n and ρ, but in both cases, the p-value is less than 0.01, signifying a highly significant degree of correlation, except for the thinnest samples.

3.4. Correlation between THz optical parameters and local density measured by X-ray

After the initial comparison of THz data averaged per sample with overall density, the analysis delves deeper, examining the data at a local, pixel-by-pixel level, using X-ray density maps. Fig. 9 presents a correlation matrix between the density, optical index, absorption coefficient, and thickness of the samples for each pixel within every sample. Given the substantial number of data points (683,100), the plots are represented in the form of kernel density estimation. The upper right panel indicates that all four properties exhibit significant correlations (p-value less than 0.001). The two parameters with the strongest correlation are density and the optical index, with an R^2 of 0.24, closely followed by density and the absorption coefficient, with an R^2 of 0.23. Regarding the absorption coefficient, it is possible to observe that many elements have values very close to zero, regardless of the values of ρ or n. However, it becomes clear that the thinnest samples, those between 1 and 3 mm in thickness, harbor most pixels with nearly zero absorption coefficient values. This observation reaffirms that, as noted previously, thickness significantly affects the THz optical parameters ($R^2 = 0.04$ for n, and $R^2 = 0.09$ for α).

To go further, for each sample, correlation coefficients and p-values were calculated between ρ and n, and ρ and α. The average R^2 between ρ and n is 10.4 % for the diverse sample group, and 7.1 % for the tropical sample group. Similarly, the R^2 values between ρ and α are 5.3 % and 7.8 %, respectively. The p-values indicate that, among the 110 samples,

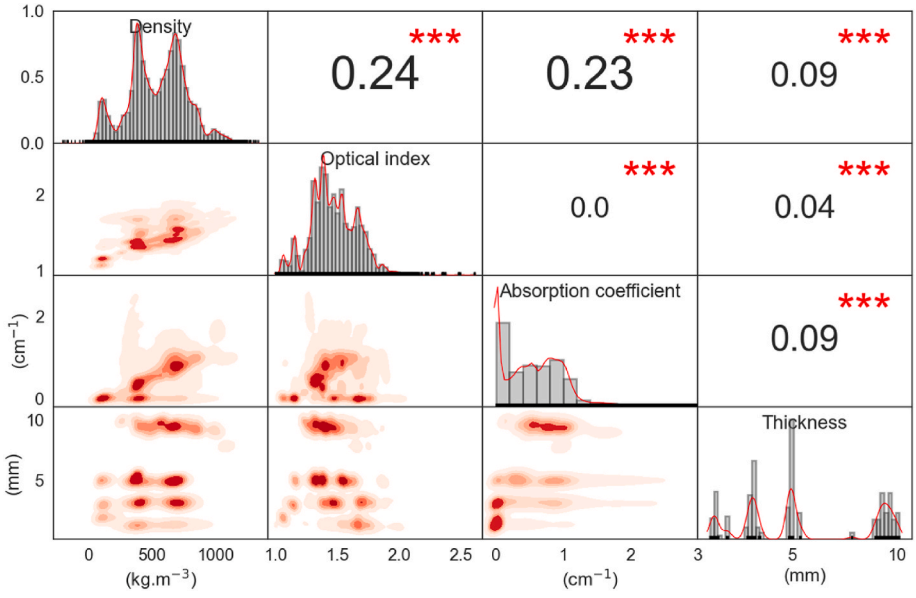

Fig. 9. Pairwise relationships between density, optical index, absorption coefficient, and sample thickness. Kernel density estimation plots are used to visualize the data distribution. The distribution of each variable is displayed on the histograms on the diagonal panels. Correlation coefficients are given in the upper right panel, with the significance in upper case (*** for $p < 0.001$, ** for $p < 0.01$, and * for $p < 0.05$).

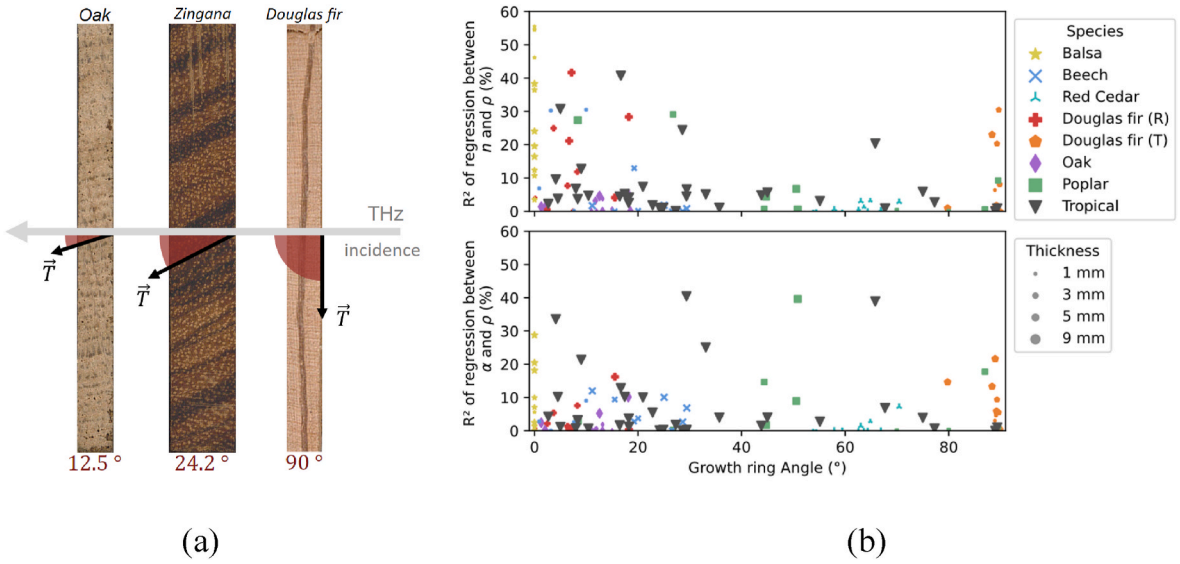

Fig. 10. (a) Growth ring angle: angle between tangential direction of wood ($\vec{T}$) and direction of wave incidence, (b) R^2 of linear regression between n and ρ, and between α and ρ, for each sample, as a function of growth ring angle.

104 demonstrate a significant level of correlation ($p < 0.1$) between ρ and n, and 98 between ρ and α. While these findings suggest a certain level of correlation between the two measurement types, it remains too imprecise to establish a robust quantitative relationship.

This imprecision can be attributed to several factors, some of which have been discussed previously: edge effects, interactions among wood fibers and THz wave polarization, sample thickness approaching the wavelength, and the inclination of growth rings. In essence, these potential factors collectively suggest that, once again, the THz beating signal modeling, at least in the context of the studied samples, is not entirely realistic. The inclination of growth rings influences the THz measurement because in the signal modeling, the medium traversed up to the metal plate is assumed to be uniform. However, when the growth rings are not perfectly radial, the density variations between earlywood and latewood disrupt this uniformity which contradicts our initial hypothesis. Fig. 10-(b) visualizes the effect of growth ring angle, as defined in Fig. 10-(a), on the correlation coefficients. For the regression with α, the angle appears to exert little influence, whereas for the regression between ρ and n, samples with less inclined growth rings, or those that are tangential, exhibit better R^2.

3.5. Multiple linear regression

Comparing the parameters pairwise did not yield excellent results, the prediction of density was conducted through multiple linear regression (MLR). Following the approach taken by Kashima et al. [20], MLR was conducted using optical index and absorption coefficient as the objective variables. Furthermore, given the prior observation that thickness (d) had a role in THz outcomes, this variable was integrated with the others in a secondary MLR. The results of these regressions are summarized in Table 2. Initially, it is obvious that incorporating thickness into the variables moderately enhances the prediction, although it remains far less robust compared to Kashima et al.'s model [20] (with an R^2 of 97.0 % as opposed to 43.8 % and 51.6 % in this instance). Additionally, the Root Mean Square Error (RMSE) closely aligns with the data's standard deviation, implying that the model struggles to efficiently explain or encapsulate the inherent data dispersion.

Table 2
Result of the prediction of density by multiple linear regression.

	Density range (kg.m^{-3})	Standard deviation (kg.m^{-3})	R^2 (%)	RMSE (kg.m^{-3})
$\rho = f(n, \alpha)$	50–1320	226	43.8	169
$\rho = f(n, \alpha, d)$			51.6	157

3.6. Discussions

The objective of this study was to investigate whether wood density measurement using THz FMCW radar could be approached in a similar manner as it is with X-ray, meaning by assuming the medium through which the wave passes is uniform, without considering anything beyond the thickness of this medium. While this approach works perfectly well for X-ray, notably due to their nanometer-scale wavelengths, previous results indicate that it's not so straightforward when dealing with THz waves. Indeed, the model employed does not accurately reflect reality, and this is for several reasons:

- Wood vessels, when voluminous enough, may scatter THz rays. This is the case for oak samples and most of the tropical samples,
- Most of the samples aren't collected from a perfect radial cut, which means that growth rings are not collinear with the THz direction of incidence. Early and latewood have different properties, the wave therefore passes through an inhomogeneous medium,
- Edge effect can occur when the THz spot (Ø ~2 mm) is at the border between earlywood and latewood,
- As wood is a birefringent material, the angle between the THz polarization direction and the fiber orientation has an influence on the measurement. However, not all the samples had their fibers perfectly aligned with the x direction, and therefore with the polarization of the wave,
- Variations in moisture content levels among the different samples, even minor ones (3.7 %), likely have an impact on the THz measurements, which are not considered in the calculations.

The diversity within the wood, particularly among the measured samples, consequently gives rise to interactions with significant consequences that were initially assumed to be less influential. Furthermore, in contrast to X-ray measurements, THz measurements are performed here through reflection, meaning the wave passing through the sample traverses it at least twice before being detected, thereby amplifying

potential disturbances.

Further research is warranted to develop a more comprehensive model that can account for these complexities and provide a more precise estimation of wood properties based on THz radar measurements.

4. Conclusion

To sum up, the potential of Terahertz Frequency Modulated Continuous Wave radar for local wood density measurement was investigated in this study, on 110 samples of varying thickness and species. This was done by modeling the beating signal and extracting the optical parameters (the optical index and the absorption coefficient) of the medium traversed, considered as uniform, as in the case of X-ray density measurement. The density mappings obtained by X-ray were used as reference values for comparison with the THz optical parameters obtained for every mm^2 of each sample. Pairwise comparisons of each parameter and a multiple linear regression indicate that the optical index and the absorption coefficient are clearly correlated with density. However, it was found that this approach presents unique challenges. Various factors, due to wood, its structure and variability, were found to interact with Terahertz waves in ways that were not initially accounted for. These findings indicate that the THz beating signal model, in its current form, may not fully capture the complexities present in most wood samples.

In conclusion, while great promise exists for wood density measurement using Terahertz FMCW radar due to its non-ionizing and non-destructive nature, the complexities introduced by wood variability and its unique interactions with Terahertz waves necessitate further investigation in this field. Future research may focus on model refinement, accounting for the intricacies of wood properties, and addressing the challenges identified in this study. Ultimately, unlocking the full potential of Terahertz technology in wood density measurement could offer a safer and non-destructive alternative to X-ray methods.

CRediT authorship contribution statement

Caroline Marc: Writing – original draft, Methodology, Data curation, Conceptualization. **Bertrand Marcon:** Writing – review & editing, Supervision. **Louis Denaud:** Writing – review & editing, Supervision. **Stéphane Girardon:** Writing – review & editing, Supervision.

Declaration of competing interest

The authors declare that they have no known competing financial interests or personal relationships that could have appeared to influence the work reported in this paper.

Acknowledgement

This study is funded by the ANR-21-CE43-0008-02 BOOST project. The authors also thank Michel Badin for providing the xylotheque used in this study, and the technical platform Xylomat of the scientific network Xylomat financed by the ANR-10-EQPX-16 XYLOFOREST which was largely used to carry out this study.

Data availability

Data will be made available on request.

References

[1] Guitard D. Mécanique du matériau bois et composites. Cépaduès. 1987.
[2] Mwaikambo LY, Ansell MP. The determination of porosity and cellulose content of plant fibers by density methods. J Mater Sci Lett 2001;20:2095–6.
[3] Baar J, Tippner J, Gryc V. The influence of wood density on longitudinal wave velocity determined by the ultrasound method in comparison to the resonance longitudinal method. Eur J Wood Wood Prod Sep. 2012;70(5):767–9. https://doi.org/10.1007/s00107-011-0550-2.
[4] Mascarenhas ARP, et al. Ultrasound to estimate the physical-mechanical properties of tropical wood species grown in an agroforestry system. Holzforschung Oct. 2021;75(10):879–91. https://doi.org/10.1515/hf-2020-0249.
[5] Marchetti B, Munaretto R, Revel G, Tomasini EP, Bianche VB. Non-contact ultrasonic sensor for density measurement and defect detection on wood. In: Proc. 16th world conference on nondestructive testing; 2004.
[6] Van Duong D, Hasegawa M, Matsumura J. The relations of fiber length, wood density, and compressive strength to ultrasonic wave velocity within stem of Melia azedarach. J. Indian Acad Wood Sci. Jun. 2019;16(1):1–8. https://doi.org/10.1007/s13196-018-0227-0.
[7] Schimleck L, et al. Non-destructive evaluation techniques and what they tell us about wood property variation. Forests Aug. 2019;10(9):728. https://doi.org/10.3390/f10090728.
[8] Berndt H, Schniewind AP, Johnson GC. High-resolution ultrasonic imaging of wood. Wood Sci Technol Jun. 1999;33(3):185–98. https://doi.org/10.1007/s002260050107.
[9] Bergsten U, Lindeberg J, Rindby A, Evans R. Batch measurements of wood density on intact or prepared drill cores using x-ray microdensitometry. Wood Sci Technol Oct. 2001;35(5):435–52. https://doi.org/10.1007/s002260100106.
[10] Davis J, Wells P. Computed tomography measurements on wood. Ind Metrol 1992;2(3–4):195–218.
[11] Decoux V, Varcin E, Leban J-M. Relationships between the intra-ring wood density assessed by X-ray densitometry and optical anatomical measurements in conifers. Consequences for the cell wall apparent density determination. Ann For Sci Apr. 2004;61(3):251–62. https://doi.org/10.1051/forest:2004018.
[12] Freyburger C, Longuetaud F, Mothe F, Constant T, Leban J-M. Measuring wood density by means of X-ray computer tomography. Ann For Sci Jan. 2009;66(8). https://doi.org/10.1051/forest/2009071.
[13] Vander Vorst A, Rosen A, Kotsuka Y. RF/microwave interaction with biological tissues. John Wiley Sons; 2006.
[14] Gagna G, Ganem Y. Effets biologiques et sanitaires des rayonnements non ionisants. 25/01 2011.
[15] Garet F, Coutaz J-L. Ondes électromagnétiques térahertz - Principes et techniques. Phys Chim Aug. 2021. https://doi.org/10.51257/a-v2-af3254.
[16] Koch M, Hunsche S, Schuacher P, Nuss MC, Feldmann J, Fromm J. THz-imaging: a new method for density mapping of wood. Wood Sci Technol 1998:7.
[17] Kim K-M, Lee S-J, Lee J-J. Development of portable X-ray CT system 1-evaluation of wood density using X-ray radiography. J Korean Wood Sci Technol 2006;34(1):15–22.
[18] Tanaka S, Shiraga K, Ogawa Y, Fujii Y, Okumura S. Applicability of effective medium theory to wood density measurements using terahertz time-domain spectroscopy. J Wood Sci Apr. 2014;60(2):111–6. https://doi.org/10.1007/s10086-013-1386-7.
[19] Inagaki T, Ahmed B, Hartley ID, Tsuchikawa S, Reid M. Simultaneous prediction of density and moisture content of wood by terahertz time domain spectroscopy. J Infrared Millim Terahertz Waves Nov. 2014;35(11):949–61. https://doi.org/10.1007/s10762-014-0095-7.
[20] Kashima M. Simultaneous detection of density, moisture content and fiber direction of wood by THz time-domain spectroscopy. '; 2020.
[21] Jankiraman M. FMCW radar design. Artech House; 2018.
[22] Pan M, Chopard A, Fauquet F, Mounaix P, Guillet J-P. Guided reflectometry imaging unit using millimeter wave FMCW radars. IEEE Trans Terahertz Sci Technol Nov. 2020;10(6):647–55. https://doi.org/10.1109/TTHZ.2020.3008330.
[23] Edlèn B. The refractive index of air. Metrologia 1966;2(2):71.
[24] Simpson WT. Specific gravity, moisture content, and density relationship for wood1993. General technical report FPL, GTR-76 1993;76:13. ill.; 28 cm.
[25] Bergounioux M. Mathématiques pour le traitement du signal. Dunod; 2014.
[26] Ahmad A, Roh JC, Wang D, Dubey A. Vital signs monitoring of multiple people using a FMCW millimeter-wave sensor. In: IEEE radar conference (RadarConf18); 2018. p. 1450–5.
[27] Meier E. WOOD! Identifying and using hundreds of woods worldwide. the wood database. 2015 [Online]. Available: https://www.wood-database.com/book/.
[28] Sihvola A. Mixing rules with complex dielectric coefficients. Subsurf Sens Technol Appl 2000;1(4):393–415. https://doi.org/10.1023/A:1026511515005.